Tuijin Jishu/Journal of Propulsion Technology
ISSN: 1001-4055
Vol. 46 No. 2 (2025)

Synthesis and characterization of a highly sunshine active metal sulfide modified TiO_2 photocatalyst and its multiple applications

T. Arunkumar[1] and M. Shanthi[1,]

[1, 1] *Department of Chemistry, Annamalai University, Annamalainagar 608002, Tamil Nadu, India*

Abstract:- The Ag_2S-loaded TiO_2 (Ag_2S–TiO_2) nanocatalyst was effectively synthesized via the precipitation thermal decomposition method. The catalyst was characterized using BET, FT-IR and HR-TEM studies. The photocatalytic and antioxidant applications of the prepared catalyst were reported. To evaluate its photocatalytic efficiency, the deterioration of Methylene Blue (MB) in an aqueous solution under sunlight exposure was used. Ag_2S–TiO_2 demonstrated greater efficiency than TiO_2, and Ag_2S in the mineralization of MB at pH 7. The impact of various operational parameters, including photocatalyst dosage, dye concentration, and initial pH on MB photomineralization was systematically investigated. Active species trapping experiments revealed that superoxide radical anions, followed by holes and hydroxyl radicals, play a key role in the photocatalytic deterioration of MB. COD measurements confirmed the successful mineralization of MB and the catalyst exhibited excellent reusability. The deterioration process was significantly accelerated by electron acceptors such as H_2O_2 and $K_2S_2O_8$. The kinetics of heterogeneous photocatalytic deterioration were effectively described using the Langmuir-Hinshelwood (L-H) kinetic model. The synthesized compound was further evaluated for antioxidant activity, and the results indicated that Ag_2S–TiO_2 nanocatalyst was potentially effective antioxidant agent.

Keywords*:* Ag_2S – TiO_2, MB dye, Photocatalyst, solar light, operational parameters, and Antioxidant activity.

1. Introduction

Photocatalytic deterioration is an effective method for breaking down organic pollutants [1, 2]. Nanotechnology, a multidisciplinary field in biochemical applications, focuses on developing nanocomposites and nanoparticles with enhanced antimicrobial and antioxidant properties, offering potential solutions for degenerative diseases and environmental challenges [3]. Nanocrystalline semiconductors act as photocatalysts, facilitating interfacial redox reactions due to their distinctive physicochemical characteristics, which stem from their nanoscale size and high surface-to-volume ratio. The semiconductors TiO_2, ZnO, and CdS are among the most often used for waste deterioration [4]. An essential component of environmental technology is the treatment of industrial wastewater to remove organic contaminants. A sophisticated oxidation method called heterogeneous photocatalysis has been developed to solve this problem [5, 6]. The band gap of a semiconductor governs its capacity to generate charge carriers upon exposure to solar irradiation.

Titanium dioxide (TiO_2) is a widely used semiconductor photocatalyst, valued for its high chemical stability [7], low toxicity [8], and effectiveness in breaking down organic pollutants in contaminated air and wastewater [9]. As an inexpensive, non-toxic, and environmentally friendly material, TiO_2 is an excellent choice for photocatalytic hydrogen (H_2) production and environmental applications, such as wastewater treatment. However, TiO_2 exhibits photocatalytic activity predominantly in the near-ultraviolet region, utilizing less than 5% of the available solar radiation [10]. To overcome this limitation, extensive research has been dedicated to modifying TiO_2 to accelerate its light absorption and improve photocatalytic performance under visible light. The valence band of TiO_2 develops holes (h^+) when electrons (e^-) in the valence band gain energy and migrate to the

conduction band when exposed to light with a wavelength of < 387 nm. These electron-hole pairs (e^-–h^+) then interact with surrounding molecules, producing highly reactive oxidizing agents, including superoxide radicals ($O_2^{\bullet-}$), hydroxyl radicals ($^{\bullet}OH$), and peroxyhydroxyl radicals ($^{\bullet}OOH$). These species facilitate the complete oxidation of several organic compounds into carbon dioxide (CO_2), water (H_2O), and other small molecules without forming intermediate byproducts [11, 12].

Silver sulfide (Ag_2S), with a direct band gap of 1.0 eV [13], is considered a promising co-catalyst for TiO_2. Several synthesis techniques, including hydrochemical bath deposition, template synthesis, sol-gel methods, microemulsion synthesis, sonochemical, hydrothermal, solvothermal, electrochemical, and microwave-assisted approaches, have been employed to fabricate nanostructured Ag_2S. The heterostructure formed enhances photocatalytic efficiency due to its synergistic effects and broad light absorption capability. However, a significant drawback of the Ag_2S-TiO_2 coupled catalyst is its low electron injection efficiency from the conduction band of Ag_2S to that of TiO_2 [14]. Additionally, the conduction band of Ag_2S (-0.3 eV) is less anodic than that of TiO_2 (−0.1 eV), while its valence band (+0.7 eV) is more cathodic compared to TiO_2 (+3.1 eV) **[15].** Moreover, Ag_2S exhibits a high absorption coefficient in the visible spectrum [16]. Due to its excellent photoelectric and thermoelectric properties, along with strong chemical stability, Ag_2S has been widely applied in optoelectronic devices, including photovoltaic cells and infrared detectors [17-19]. Furthermore, it has shown remarkable photocatalytic potential, particularly in the deterioration of pollutant dyes such as methylene blue [15, 20-22].

Dyes are organic compounds with intricate aromatic molecular structures that provide vibrant and durable colours to different materials. However, these intricate structures also make dyes highly stable and resistant to biodegradation. The extensive use of dyes frequently raises environmental concerns, especially due to the release of coloured wastewater into natural water sources [23, 24]. Advanced oxidation technologies (AOTs) present a viable alternative to traditional treatment methods by enabling the complete breakdown of organic pollutants into carbon dioxide and water. In this study, Ag_2S/TiO_2 composite photocatalysts, designed for the deterioration of organic dyes under solar light, were synthesized using a conventional hydrothermal method. The Ag_2S/TiO_2 composites exhibited distinct characteristics and properties compared to bulk Ag_2S and TiO_2. Their enhanced photocatalytic performance was evaluated by degrading methylene blue (MB) in water-based solutions under sunlight exposure, with results compared against those of pure anatase TiO_2.

2. Experimental

2.1. Materials and Methods

The commercial non-azo dye Methylene Blue dye (MB) was purchased from Aldrich. **Fig. 1** depicts the chemical structure and absorption spectrum of Methylene Blue (MB) dye**.** Silver nitrate (99%), sodium sulfide (99%) and titanium isopropoxide (99%) of AnalaR grade (Himedia), along with 2-propanol (99.5% spectroscopic grade), H_2SO_4 or NaOH, were utilized as received from Sigma Aldrich. Deionized water was utilized in the preparation of all experimental solutions.

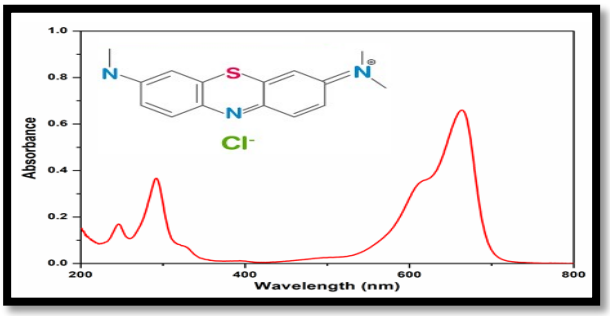

Fig. 1. The chemical structure and absorption spectrum of MB dye

2.2. Synthesis of Ag_2S-TiO_2 photocatalysts

Ag_2S-loaded TiO_2 was synthesized using a precipitation-thermal decomposition method (Scheme 1). The detailed preparation method was given in our previously reported paper [25].

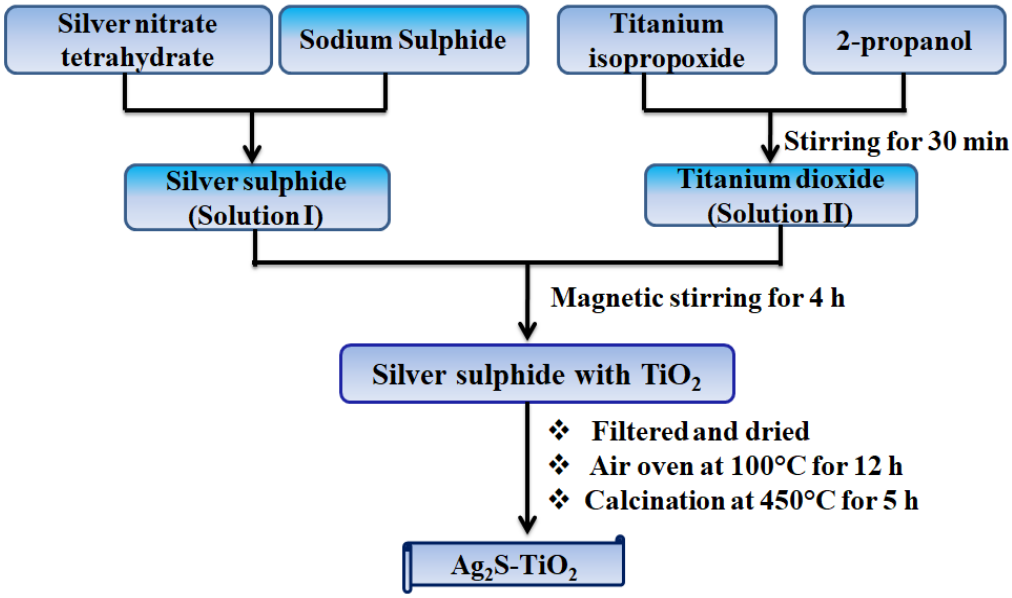

Scheme. 1. Schematic representation for preparation of Ag_2S-TiO_2

2.3. Analytical methods

The characterization of these nanocatalysts (bare TiO_2 and Ag_2S-TiO_2) was performed using various analytical methods, including XRD, FE-SEM, EDS, UV-DRS, PL, and XPS, and the details are provided in our previously published paper [25]. The remaining analyses (BET, FT-IR and HR-TEM) are presented in this manuscript.

2.4. Photodeterioration experiment

Solar photocatalytic deterioration experiments were conducted under controlled conditions during peak sunlight hours, specifically between 11:00 a.m. and 2:00 p.m. on clear days. The reaction was carried out in a borosilicate glass tube reactor with a volume of 50 mL, a height of 40 cm, and an internal diameter of 12.6 mm. Approximately 50 mL of MB dye (3×10^{-4} M) was combined with a suitable quantity of nanocatalysts in the dark for 30 minutes before being exposed to direct sunlight. No solvent volatility was detected throughout the illumination period. At specified time intervals, 2–3 mL samples were removed and each sample was appropriately diluted before a UV-visible spectrophotometer was used to track variations in the concentration of the MB dye based on its characteristic absorbance at 291.5 nm.

2.5. Solar radiation intensity readings

Solar radiation intensity was monitored at 30-minute intervals and the average intensity for each experiment was determined. The sensor was consistently positioned to capture the highest intensity readings. The measurements were conducted using an LT Lutron LX-10/A Digital Lux Meter, with recorded intensities were 1250 ± 100 lux, which remained relatively stable throughout the experiments.

2.6. Characterization techniques

The catalysts' specific surface areas were determined using a Micromeritics ASAP 2020 sorption analyzer. Before analysis, the samples were degassed at 423 K for 12 hours. Measurements were performed at 77

K with nitrogen (N_2) gas as the adsorbate. The specific surface area was calculated using the Brunauer–Emmett–Teller (BET) multipoint method with a least-squares fitting approach. The nanocatalyst's configuration and crystallinity were analyzed using a high-resolution transmission electron microscope (HR-TEM), with samples dried naturally and analyzed on a JEOL 2100+ HR-TEM. Fourier transform infrared (FT-IR) spectra were monitored using a spectrometer with KBr pellet holders and UV-visible spectra were measured using a SHIMADZU UV 2600 PC UV-visible spectrophotometer.

2.7. Chemical oxygen demand (COD) measurements

The chemical oxygen demand (COD) technique was employed to determine the amount of oxygen consumed during the reaction in the solution. The dye solution was refluxed for 2 hours with $HgSO_4$, a measured volume of standard $K_2Cr_2O_7$, Ag_2SO_4, and H_2SO_4. Following reflux, the solution was titrated with standard ferrous ammonium sulfate (FAS) using ferroin as the indicator. A blank sample, prepared using the same procedure but without the dye, was also titrated. COD values were then calculated using the corresponding Eqn. 1.

$$\text{COD} = \frac{(\text{Blank titre value} - \text{dye sample titre value}) \times \text{normality of FAS} \times 8 \times 1000}{\text{Volume of the sample}} \quad (1)$$

3. Results and Discussion

3.1. Primary analysis

Various weight percentages of Ag_2S-TiO_2 nanocatalyst were used to study the deterioration of MB dye under solar light irradiation, with the results summarized in **Table.1.** The data indicate that as the Ag_2S content increased, the deterioration efficiency of MB also improved, reaching a maximum of 7.0 wt%. Beyond this point, further increases in Ag_2S loading led to a decline in deterioration efficiency. The optimal Ag_2S content for effective MB dye removal was determined to be 7.0 wt%, making this composition the focus of subsequent studies and characterization.

Table.1. Effect of different wt% of Ag_2S for the MB dye deterioration under solar light

Wt % of Ag_2S	% of MB dye deterioration
2.5	72.6
4.8	81.4
7.0	89.8
9.2	71.8
11.2	59.7

[MB] = 3×10^{-4} mol/L, catalyst suspended = 2 g/L, pH = 7, airflow rate = 8.1 mL s^{-1}, irradiation time = 40 min.

3.2. BET analysis

The surface area of the catalyst plays a critical role in determining its reactivity. The surface area of the Ag_2S-TiO_2 nanocatalyst was determined using the nitrogen gas adsorption technique. The N_2 adsorption-desorption isotherms of both bare TiO_2 and Ag_2S-TiO_2 exhibit a type II hysteresis loop. The corresponding pore size distributions for bare TiO_2 and Ag_2S-TiO_2 are illustrated in the insets of **Fig. 2a, b. Table.2** summarizes the BET surface area and pore volume data for both samples. Notably, Ag_2S-TiO_2 nanocatalyst possesses a significantly higher BET surface area of 211.917 m^2/g compared to bare TiO_2, which has a surface area of 109.993 m^2/g.

Table.2. Surface properties of bare TiO_2 and Ag_2S-TiO_2 nanocatalysts

Properties	Bare TiO_2	Ag_2S-TiO_2 nanocatalyst
BET surface area	109.993 $m^2\ g^{-1}$	211.917 $m^2\ g^{-1}$
Total pore volume	0.30 $cm^3\ g^{-1}$	0.43 $cm^3\ g^{-1}$

3.3. Fourier Transform-Infrared (FT-IR) Spectroscopy

The FT-IR spectra of TiO_2 and Ag_2S-TiO_2 nanocatalysts, shown in **Fig. 3**, exhibit distinct peaks corresponding to oxygen-containing functional groups. The bending vibrations of O-H groups are notably observed at 1627 cm^{-1} [26–28]. Furthermore, the broad absorption band at 3431 cm^{-1} is ascribed to the O-H stretching vibration of adsorbed water (H_2O) on the surface of the Ag_2S-TiO_2 nanocatalyst, indicating the presence of surface-bound water, which is common in catalysts exposed to ambient moisture. Additionally, low-frequency bands related to Ti-O-Ti bonds appear around 696 cm^{-1}, while the strong peak at 3431 cm^{-1} in both TiO_2 and Ag_2S-TiO_2 nanocatalyst is also assigned to O-H stretching vibrations.

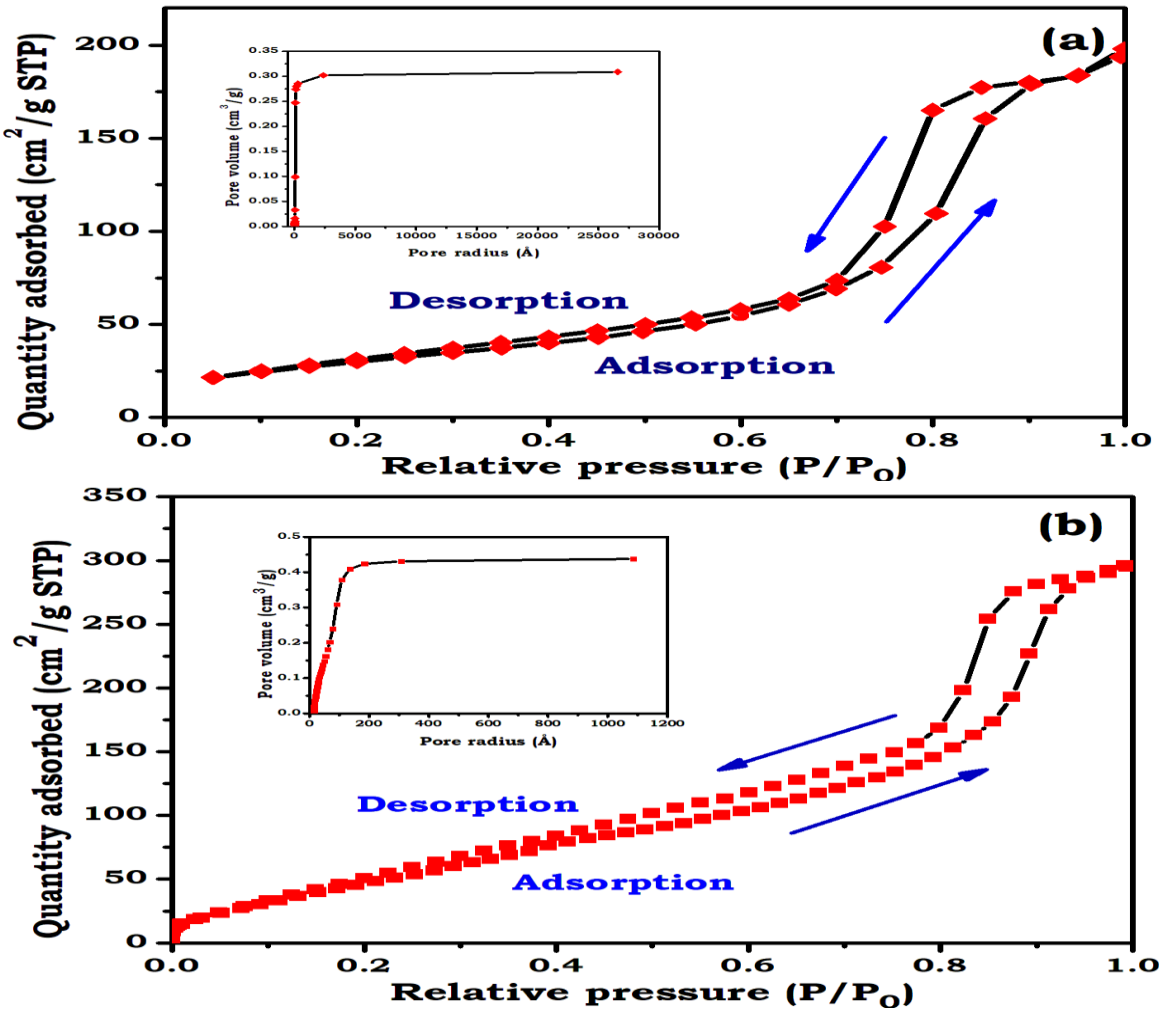

Fig. 2. N_2 adsorption-desorption isotherm of a) bare TiO_2 and b) Ag_2S-TiO_2. Inset shows pore size distribution

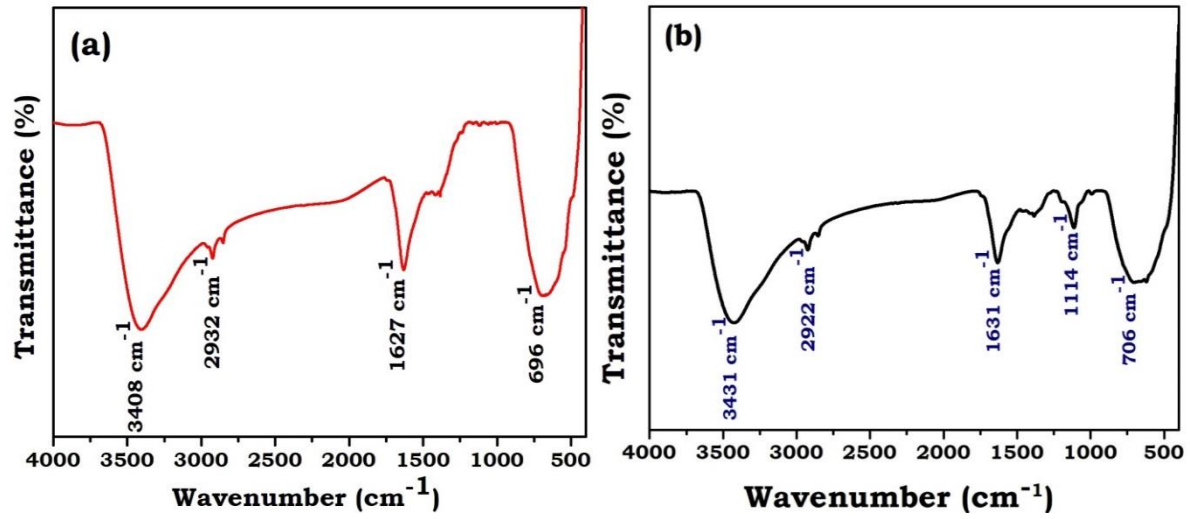

Fig. 3. FT-IR spectra of (a) bare TiO_2 and (b) Ag_2S-TiO_2 nanocatalysts

3.4. HR-TEM Analysis

The surface morphology of the synthesized Ag_2S-TiO_2 nanocatalyst is illustrated in **Fig. 4(a–e). Fig. 4(a–b)** depicts the structure of Ag_2S-TiO_2 nanocatalyst, composed of numerous small dark particles. **Fig. 4(c–d)** highlight selected Ag_2S-TiO_2 nanocatalyst, confirming their polycrystalline anatase nature with randomly oriented small crystals. The Ag_2S particles are uniformly distributed on the TiO_2 surface, predominantly exhibiting a circular or spherical shape. The SAED pattern of TiO_2, shown in **Fig. 4(e)**, corresponds to various crystallographic planes and reveals distinct diffraction rings, confirming crystallinity. HR-TEM images captured at both low and high magnifications reveal that the anatase TiO_2 and Ag_2S particles exhibit monodispersity and maintain a consistent size distribution. The analysis further confirms the crystal structure, revealing interplanar spacings of 2.08 nm and 2.58 nm for TiO_2 (corresponding to the (200) and (022) planes) and 3.08 nm and 3.88 nm for Ag_2S (corresponding to the (111) and (002) planes).

3.5. Photocatalytic Activity Investigations

The remaining percentage of MB dye after solar light exposure to an aqueous MB solution (3×10^{-4} M), both with and without a photocatalyst, is depicted in **Fig. 5.** When Ag_2S-TiO_2 was used as the photocatalyst, 89.8% of the dye deteriorated after 40 minutes of solar irradiation (curve a). In contrast, the Ag_2S-TiO_2 nanocatalyst resulted in a 55.3% reduction in dye concentration without solar light (curve c), likely due to dye adsorption onto the catalyst's surface. Minimal deterioration (0.9%) was observed under solar exposure without a catalyst (curve b). These findings highlight the essential role of both the photocatalyst and solar light in achieving effective dye deterioration. Under comparable conditions, deterioration rates of 27.5% (curve d) and 54.2% (curve e) were obtained using synthesized Ag_2S and TiO_2 as photocatalysts, respectively. This indicates that the solar/Ag_2S-TiO_2 nanocatalyst is the most efficient among the tested photocatalysts for degrading MB dye.

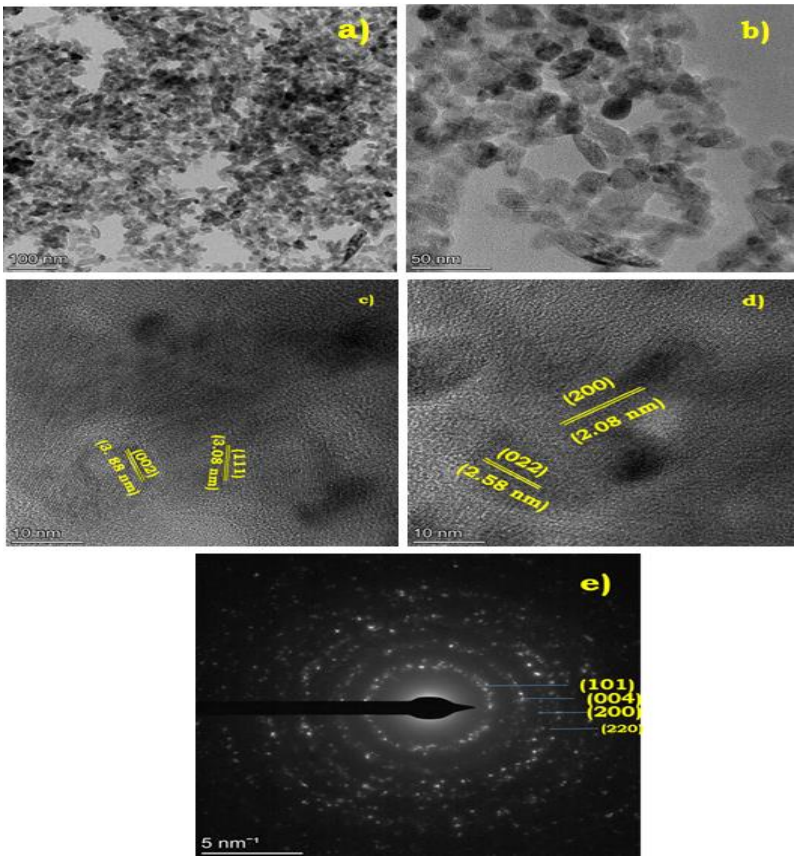

Fig. 4. HR-TEM analysis of Ag_2S-TiO_2 nanocatalyst

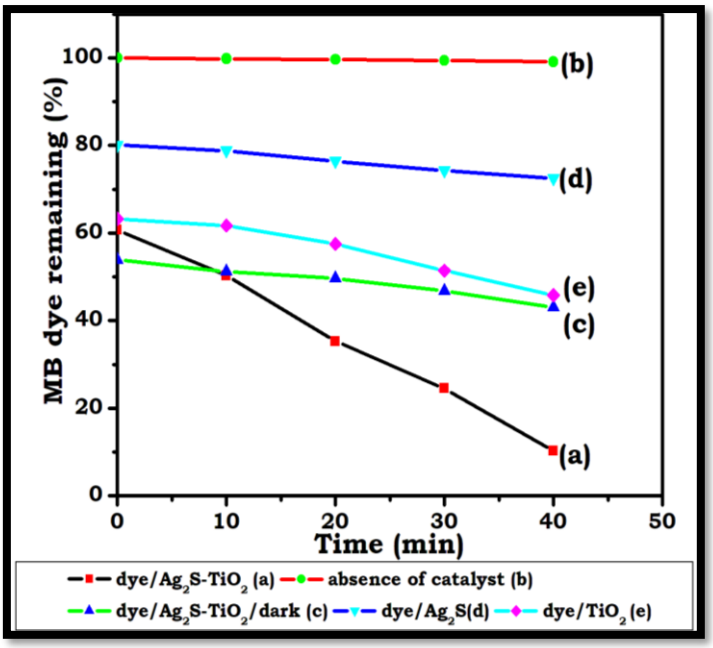

Fig. 5. Photodegradability of MB dye under solar light: [MB] = 3×10^{-4} mol/L, pH = 7.0±0.1, 7.0 wt% Catalyst suspended = 2 g/L, I_{solar} = 1250×100±100 lux, airflow rate = 8.1 mLs^{-1}.

3.6. Influence of the operational parameters

3.6.1. Impact of pH

The pH of the solution plays a key factor influencing the photocatalytic deterioration of diverse pollutants **[29, 30].** The impact of pH on the photodeterioration of MB was examined inside a pH range of 3–11, as illustrated in **Fig. 6.** The results indicate that increasing the pH from 3 to 7 enhances the removal efficiency of MB, after which it declines. The optimal pH for effective MB deterioration using Ag_2S-TiO_2 is 7. Lower removal efficiency in acidic conditions is attributed to the dissolution of TiO_2, as it reacts with acids at low pH levels. At higher pH values, the Ag_2S-TiO_2 nanocatalyst becomes negatively charged due to the adsorption of OH^- ions. The formation of hydroxyl radicals ($OH^•$) is promoted by the concentration of OH^- ions in the reaction medium and at the particle interface. An experiment was conducted to evaluate the dark adsorption of MB at varying pH levels, as photocatalytic performance is influenced by dye molecule adsorption. After 30 minutes of adsorption equilibrium, the adsorption rates at different pH levels 3, 5, 7, 9 and 11 were recorded as 31%, 41.2%, 55.3%, 23.7%, and 19.3% respectively. The highest adsorption was observed at pH 7, indicating that deterioration is most effective under this condition.

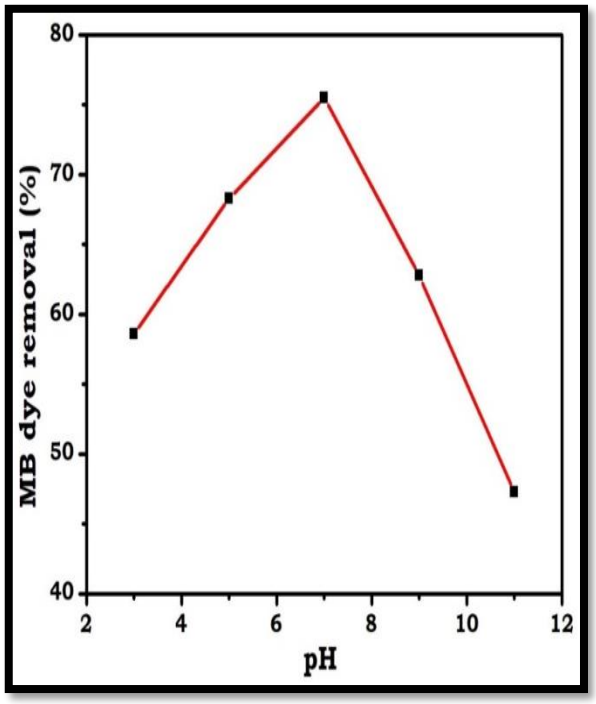

Fig. 6. Effect of initial pH on the deterioration of MB using solar light/Ag_2S-TiO_2 nanocatalyst: [MB] = 3×10^{-4} mol/L, 7.0 wt% Catalyst suspended = 2 g/L, I_{solar} = 1250×100±100 lux, airflow rate = 8.1 mL s^{-1}, irradiation time = 30 min.

3.6.2. Impact of the catalyst

The catalyst concentration was adjusted from 0.5 to 3 g/L in a series of experiments to determine the optimal catalyst loading **(Fig. 7).** After 30 minutes of radiation exposure, catalyst loadings within this range were analyzed. Notably, the rate constant for MB deterioration increased as the catalyst concentration rose from 0.5 to 2 g/L but declined with further increases. The enhancement in deterioration rate is attributed to (i) the increased amount of catalyst, which enhances dye molecule adsorption, and (ii) the higher density of catalyst particles within the illuminated region. However, at concentrations above 2 g/L, the deterioration efficiency decreases due to light scattering and reflection by excess catalyst particles **[31, 32].**

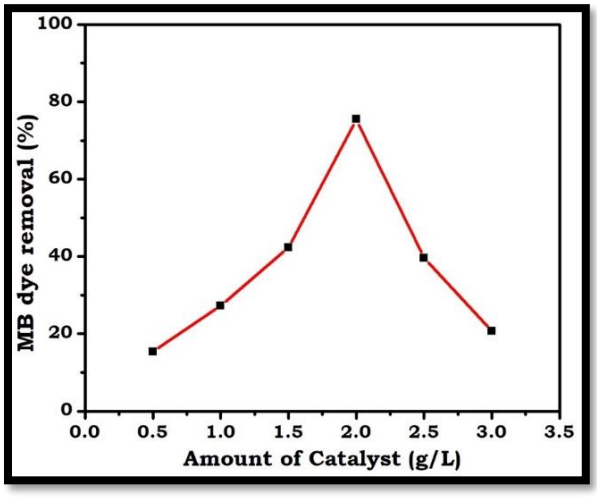

Fig. 7. Effect of catalyst weight on the photocatalytic deterioration of MB using solar light: [MB] = 3×10^{-4} mol/L, pH = 7.0±0.1, I_{solar} = 1250×100±100 lux, airflow rate = 8.1 mLs^{-1}, time = 30 min.

3.6.3. Impact of starting dye concentration

The impact of different initial dye concentrations on MB deterioration over the Ag_2S-TiO_2 nanocatalyst was examined. As the dye concentration increased from 1 to 5 × 10^{-4} M, the deterioration efficiency declined **(Fig. 8).** Throughout the experiments, both the catalyst dosage and light intensity were kept constant for all initial dye concentrations. As the production of hydroxyl radicals remains unaffected, the variation in dye molecules available for interaction with these radicals leads to a decline in their interactions. Additionally, at higher initial dye concentrations, the photon penetration depth into the solution is reduced.

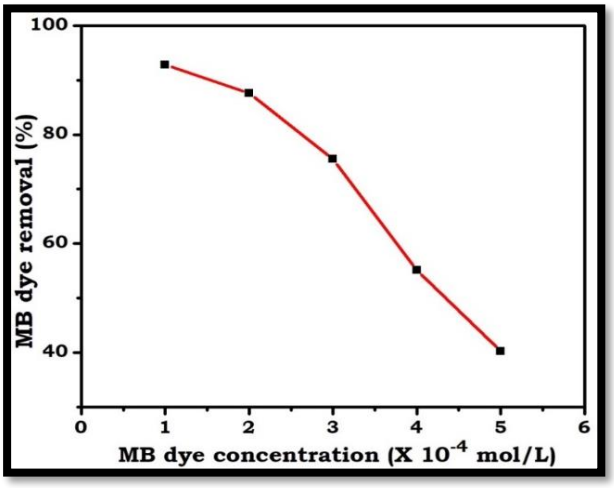

Fig. 8. Effect of various initial dye concentrations on the deterioration of MB using solar light/Ag_2S-TiO_2 nanocatalyst: pH = 7.0±0.1, 7.0 wt% Catalyst suspended = 2 g/L, I_{solar} = 1250×100±100 lux, airflow rate = 8.1 mL s^{-1}, time = 30 min.

3.7. Effect of oxidants

3.7.1. Impact of H_2O_2

The impact of H_2O_2 addition on photocatalytic oxidation is shown in **Fig. 9a.** An addition of around 5 mmol of H_2O_2 increased the deterioration rate from 75.5% to 82.2% within 30 minutes. The capture of photogenerated electrons from the conduction band by H_2O_2 suppresses electron-hole recombination while

simultaneously facilitating the generation of hydroxyl radicals (Eq. 2). These hydroxyl radicals are essential for the breakdown of pollutants **[33].** However, when the H_2O_2 dosage exceeds 5 mmol, the deterioration rate drops due to the scavenging effect of H_2O_2 on hydroxyl radicals. Excess hydrogen peroxide reacts with hydroxyl radicals ($^{\bullet}OH$) to form hydroperoxy radicals ($^{\bullet}HO$) (Eq. 3, 4). These radicals exhibit significantly lower reactivity and have a minimal impact on the oxidation of the dye **[34].**

$$e^-_{(CB)} + H_2O_2 \longrightarrow {}^{\bullet}OH + OH^- \quad (2)$$

At higher dosage,

$$H_2O_2 + {}^{\bullet}OH \longrightarrow HO_2{}^{\bullet} + H_2O \quad (3)$$

$$HO_2{}^{\bullet} + {}^{\bullet}OH \longrightarrow H_2O + O_2 \quad (4)$$

3.7.2. Impact of $K_2S_2O_8$

To investigate the photocatalytic deterioration of MB dye, the $K_2S_2O_8$ dosage was adjusted from 5 to 20 mg per 50 mL, as depicted in **Fig. 9b.** The addition of $K_2S_2O_8$ up to 10 mg enhanced deterioration from 75.5% to 84.5% after 30 minutes; however, further increases in dosage (above 10 mg) led to a reduction in deterioration efficiency **[35, 36].** The sulfate radical anion ($SO_4^{\bullet-}$) is a key factor in the deterioration process, as it can react with both photogenerated electrons and water molecules to produce hydroxyl radicals (Eq. 5-7). At higher doses of $S_2O_8^{2-}$, the deterioration rate slows due to an increase in SO_4^{2-} ions. These excess SO_4^{2-} ions adsorb onto the TiO_2 surface, diminishing the catalyst's activity.

$$S_2O_8^{2-} + e^-_{(CB)} \longrightarrow SO_4^{\bullet-} + SO_4^{2-} \quad (5)$$

$$SO_4^{\bullet-} + e^-_{(CB)} \longrightarrow SO_4^{2-} \quad (6)$$

$$SO_4^{\bullet-} + H_2O \longrightarrow {}^{\bullet}OH + SO_4^{2-} + H^+ \quad (7)$$

3.7.3. Impact of Na_2CO_3

Fig. 9c illustrates the effect of Na_2CO_3 on the photocatalytic deterioration of MB. The study revealed that increasing the amount of Na_2CO_3 decreases the removal efficiency. The results show that adding Na_2CO_3 (up to 20 mg) reduces the removal rate from 75.5% to 26.5% after 30 minutes **[37].** As the concentration of carbonate ions increases, the hydroxyl radicals gradually decrease, significantly hindering the photocatalytic deterioration process (Eq. 8).

$$CO_3^{2-} + {}^{\bullet}OH \longrightarrow OH^- + CO_3{}^{\bullet-} \quad (8)$$

3.7.4. Impact of NaCl

The deterioration of MB was studied using NaCl, as shown in **Fig. 9d.** The addition of Cl^- ions (up to 20 mg) to the reaction solution caused the deterioration rate to decrease from 75.5% to 40.8% after 30 minutes. This reduction in deterioration efficiency was attributed to the hole-scavenging ability of chloride ions (Eq. 9), where the dye molecules compete with the chloride ions for the available holes in the reaction **[38].**

$$Cl^- + h^+_{(VB)} \longrightarrow Cl^{\bullet} \quad (9)$$

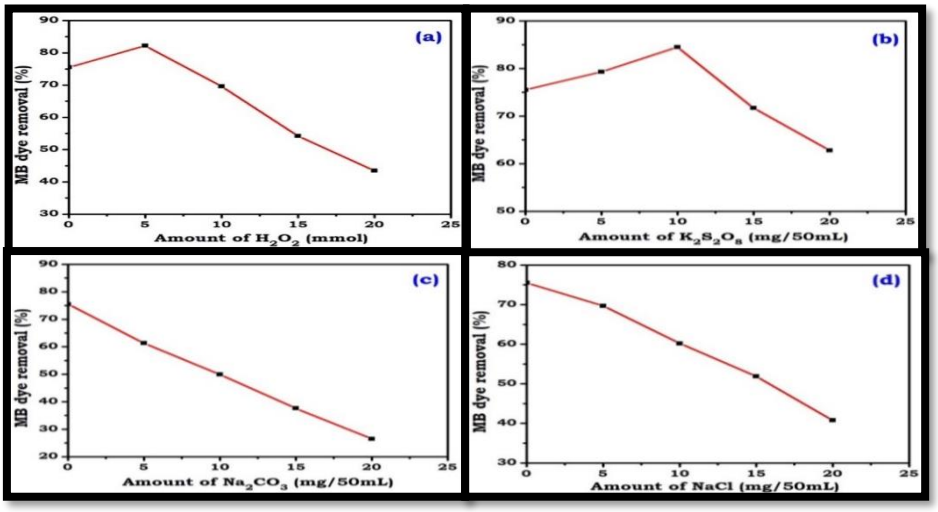

Fig. 9. Effect of additives on the deterioration of MB using solar light/Ag_2S-TiO_2 nanocatalyst: (a) H_2O_2, (b) $K_2S_2O_8$, (c) Na_2CO_3 and (d) NaCl, pH = 7.0±0.1, 7.0 wt% Catalyst suspended = 2g/L, I_{solar} = 1250×100±100 lux, airflow rate = 8.1 mL s^{-1}, irradiation time = 30 min.

3.8. Catalyst reusability

Fig. 10 illustrates the outcomes of the recycling experiments, revealing that the catalyst retained 74.8% of its activity after four consecutive cycles of solar light irradiation. These findings confirm that the Ag_2S–TiO_2 nanocatalyst retains its efficiency and reusability under sunlight exposure.

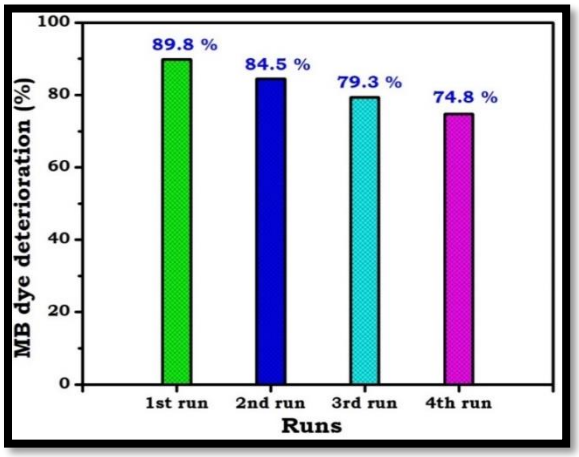

Fig. 10. Catalyst reusability: MB = 3×10^{-4} mol/L, pH = 7.0±0.1, 7.0 wt% Catalyst suspended = 2 g/L, I_{solar} = 1250×100±100 lux, airflow rate = 8.1 mL s^{-1}, irradiation time = 40 min.

3.9. Radical Scavengers Test

To demonstrate that the superoxide radical anion ($O_2^{\bullet-}$) is the primary reducing agent in the photocatalytic deterioration method, the impact of several radical scavengers, including benzoquinone, ethylenediaminetetraacetic acid (EDTA), and 2-propanol was analyzed and is presented in **Table 3**. The data indicate that photocatalytic deterioration is most effective in the without scavengers, reaching 89.8%. However, adding benzoquinone reduces the deterioration efficiency to 68.3%, suggesting that the superoxide radical anion ($O_2^{\bullet-}$) plays a crucial role in the photocatalytic decomposition. Similarly, other radical scavengers, such as 2-propanol (51.7%) and Ethylenediaminetetraacetic acid (38.9%), exhibit a comparable inhibitory effect.

Table.3. Effects of different radical scavengers on the photodeterioration of MB dye under solar radiation utilizing Ag_2S-TiO_2 nanocatalyst

Different radical scavengers	MB dye deterioration percentage (%)
Without scavenger	89.8
Benzoquinone	68.3
2-propanol	51.7
Ethylenediaminetetraacetic acid	38.9

3.9. Chemical Oxygen Demand (COD) analysis

The deterioration was assessed using COD measurements to verify the mineralization of MB. The COD reduction percentages are displayed in **Table 4.** Following 40 minutes of irradiation with Ag_2S–TiO_2 nanocatalyst, a 65.8% decrease in COD was achieved, confirming the mineralization of the dye.

Table.4. COD values and removal rate by solar light/Ag_2S-TiO_2 nanocatalyst

Time (min)	COD removal (%)
0	0
20	40.4
40	65.8

3.10. Kinetic analysis

The photocatalytic deterioration of MB dye using Ag_2S-TiO_2 nanocatalyst adhered to pseudo-first-order kinetics. The corresponding equation describes the rate expression relevant for low initial concentrations of the MB dye substrate.

$$\frac{-d[C]}{dt} = k'[C] \qquad (10)$$

Where k represented the rate constant of pseudo-first order. The deterioration rate constant is detailed in **Table 5**.

Table.5. Rate constants of photocatalytic deterioration of MB dye using solar light/Ag_2S-TiO_2 nanocatalyst

Initial concentration of dye X (10^{-4}) mol/L	Deterioration
1	0.0796
2	0.0663
3	0.0493
4	0.0378
5	0.0315

The adsorption-desorption equilibrium was established as MB dye adhered to the surface of the Ag_2S-TiO_2 nanocatalyst. The initial condition for the kinetic analysis was the equilibrium concentration of MB dye, determined through the adsorption process. By integrating Equation 10 and assuming $C=C_0$,at t=0, Equation 11 was derived.

$$\ln\left[\frac{C_o}{C}\right] = k't \qquad (11)$$

C_0 represented the initial concentration of MB, while C denoted the concentration at any given time. The rate constant for ln (C_0/C) was plotted against the deterioration time, as shown in **Fig. 11a.** The concentration of MB dye exhibited a linear correlation with irradiation time. The Langmuir-Hinshelwood (L-H) kinetic model, commonly applied in heterogeneous photocatalytic reactions **[39, 40],** was adapted to reflect the solid-liquid interaction **[41],** which aligned with the experimental findings. The rate of MB deterioration was governed by the adsorption of MB onto the Ag_2S-TiO_2 s nanocatalyst **[42].** The impact of dye concentration on the rate of deterioration was described by the following equations (Eq. 12, 13).

$$r = \frac{K_1 K_2\, C}{1 + K_1 C} \qquad (12)$$

$$\frac{1}{r} = \frac{1}{K_2 K_1 C} + \frac{1}{K_2} \qquad (13)$$

Where 'C' denotes the MB concentration at time't', with K_1 representing the adsorption constant and K_2 corresponding to the reaction characteristics of the MB substrate. The effectiveness of the Langmuir-Hinshelwood (L-H) equation in facilitating dye deterioration is evidenced by the linear plot obtained by plotting the reciprocal of the initial rate (1/r) against the reciprocal of the initial MB concentration (1/C), as illustrated in **Fig. 11b.** The values for K_1 and K_2 were derived from the slope and intercept, yielding values of 1.1×10^3 M^{-1} and 5.9×10^{-5} $M^{-1}min^{-1}$ respectively.

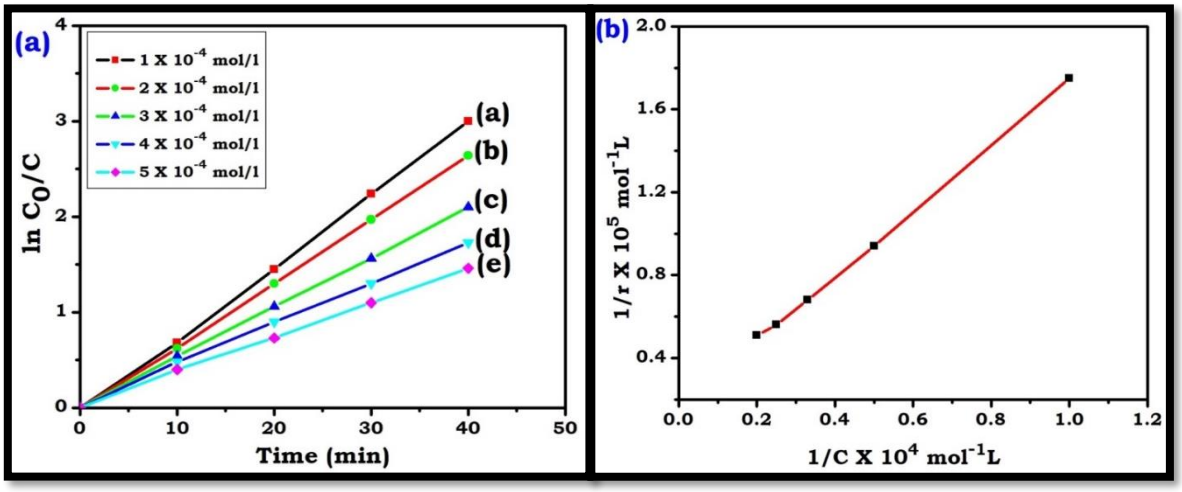

Fig. 11. (a) Kinetics of MB dye deterioration for different initial densities by solar light/Ag_2S-TiO_2 nanocatalyst: pH = 7.0±0.1, Ag_2S-TiO_2 nanocatalyst = 2 g/L, I_{solar} = 1250×100±100 lux, airflow rate = 8.1 mL $s^{-1,}$ and (b) Linearized reciprocal kinetic plot of the deterioration of MB by Ag_2S-TiO_2 nanocatalyst.

3.11. Mechanism of deterioration

The proposed mechanism for dye deterioration is based on the energy levels of Ag_2S and TiO_2 are already given in our previous paper **[25].** Upon sunlight exposure, the electrons are excited and transfer from the conduction (CB) band of Ag_2S to the CB of TiO_2, while holes migrate from the valence band (VB) of TiO_2 to VB of Ag_2S. This charge transfer occurs more efficiently than the electron-hole recombination process in Ag_2S. The electrons in the CB of TiO_2 react with O_2, contributing to dye deterioration. Simultaneously, the holes in Ag_2S, along with those generated in TiO_2 by photoexcitation, interact with H_2O and OH^- to form hydroxyl radicals ($^{\bullet}OH$), which further contribute to the breakdown of dye molecules. The equations are given below (Eqn. 14-22).

$$Ag_2S\text{–}TiO_2 + h\nu \longrightarrow Ag_2S\text{–}TiO_2\,(h^+, e^-) \qquad (14)$$

$$Ag_2S\text{–}TiO_2\,(h^+, e^-) \longrightarrow Ag_2S\,(h^+)\text{–}TiO_2\,(e^-) \qquad (15)$$

$$h^+ + OH^- \longrightarrow {}^{\bullet}OH \qquad (16)$$

$$h^+ + H_2O \longrightarrow {}^{\bullet}OH + H^+ \qquad (17)$$

$$e^- + O_2 \longrightarrow O_2^{\bullet -} \quad (18)$$

$$h^+ + OM \longrightarrow OM^{\bullet +} \quad (19)$$

$$OM^{\bullet +} + O_2 \longrightarrow \text{Products} \quad (20)$$

$$^{\bullet}OH + OM \longrightarrow \text{Products} \quad (21)$$

$$O_2^{\bullet -} + OM \longrightarrow \text{Products} \quad (22)$$

3.12. Antioxidant Activity

The antioxidant and free radical scavenging potential of the synthesized Ag_2S-TiO_2 nanocatalyst was assessed using the DPPH assay, as presented in **Fig. 12a, b.** This evaluation was based on the DPPH assay, in which the stable purple DPPH radical undergoes reduction and turns pale yellow in the presence of antioxidant compounds. The results revealed that, at all tested concentrations, vitamin C (standard) demonstrated higher radical scavenging activity compared to the synthesized nanocatalyst. The DPPH free radical scavenging activity of the samples increased with concentration, indicating a dose-dependent antioxidant effect. Notably, the Ag_2S-TiO_2 nanocatalyst exhibited greater inhibition, with an IC50 value of 37.90% at 400 µg/mL, surpassing the activity of Ag_2S and TiO_2 nanocatalyst. The enhanced antioxidant activity of the Ag_2S-TiO_2 nanocatalyst, compared to its components, can be ascribed to the synergistic interaction between silver and titanium ions, along with oxides. This suggests its potential application as a drug carrier with reduced cytotoxicity.

Concentration (µg/mL)	IC_{50} % of DPPH			
0	**Ag_2S**	**TiO_2**	**Ag_2S-TiO_2**	**Standard**
20	9.80	8.71	11.76	30.28
40	18.73	15.46	19.82	50.10
80	24.61	21.13	25.49	70.80
200	29.62	27.23	30.28	87.36
400	**35.51**	**33.33**	**37.90**	**95.42**

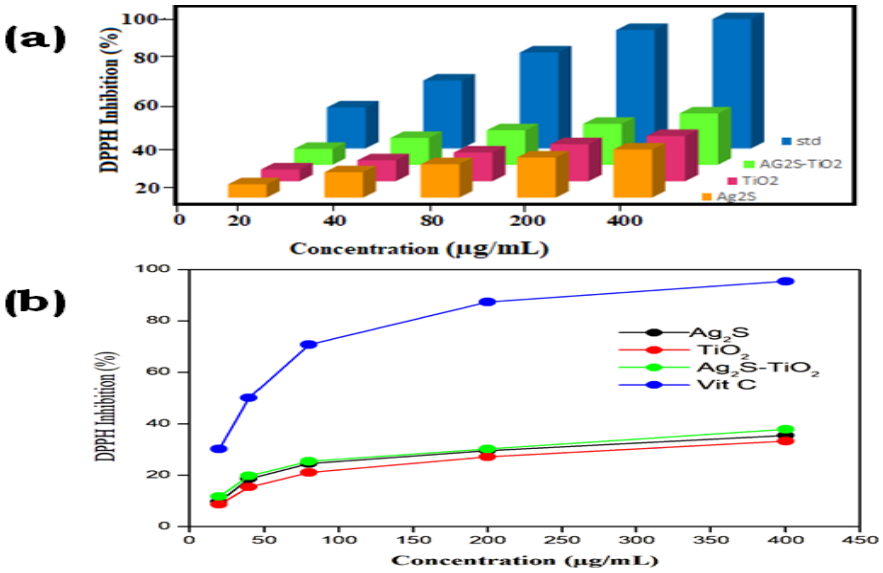

Fig.12. (a) DPPH radical scavenging activity (%) and (b) IC_{50} values of the synthesized materials (Ag_2S, TiO_2 and Ag_2S-TiO_2) and Vitamin C as standard using DPPH radical scavenging method.

Conclusion

A novel Ag_2S-loaded TiO_2 nanocatalyst was successfully synthesized using the precipitation thermal decomposition method. The presence of Ag_2S in TiO_2 was confirmed through BET, FT-IR, and HR-TEM analyses. Ag_2S–TiO_2 exhibited superior efficiency in degrading Methylene Blue (MB) under solar light irradiation compared to TiO_2, and Ag_2S. The addition of oxidants (H_2O_2 and $K_2S_2O_8$) significantly enhanced the deterioration efficiency. Optimal dye removal conditions were identified at a pH of 7 and a catalyst loading of 2 g/L. The catalyst demonstrated excellent reusability, and COD analysis confirmed the mineralization of the MB molecule. A proposed mechanism for MB deterioration further highlights the potential of the Ag_2S–TiO_2 nanocatalyst for wastewater treatment applications. The produced catalyst has high antioxidant properties.

Acknowledgement

Authors are thankful to Prof. Dr. M. Swaminathan, Emeritus professor (CSIR), Nanomaterial laboratory, Department of Chemistry, Kalasalingam Academy of Research and Education, Krishnankoil, Tamil Nadu for his valuable suggestions and help.

Refrences

[1] Reddy, P. V. L., Kim, K. H., Kavitha, B., Kumar, V., Raza, N., & Kalagara, S. (2018). Photocatalytic degradation of bisphenol a in aqueous media: A review. *Journal of environmental management*, *213*, 189-205; https://doi.org/10.1016/j.jenvman.2018.02.059.

[2] Zou, W., Gao, B., Ok, Y. S., & Dong, L. (2019). Integrated adsorption and photocatalytic degradation of volatile organic compounds (VOCs) using carbon-based nanocomposites: A critical review. *Chemosphere*, *218*, 845-859; https://doi.org/10.1016/j.chemosphere.2018.11.175.

[3] Nazem, A., & Mansoori, G. A. (2008). Nanotechnology solutions for Alzheimer's disease: advances in research tools, diagnostic methods and therapeutic agents. *Journal of Alzheimer's disease*, *13*(2), 199-223; DOI: 10.3233/JAD-2008-13210.

[4] Linsebigler, A. L., Lu, G., & Yates Jr, J. T. (1995). Photocatalysis on TiO_2 surfaces: principles, mechanisms, and selected results. *Chemical reviews*, *95*(3), 735-758; https://doi.org/1 0.1021/cr00035a013.

[5] Chatterjee, D., & Dasgupta, S. (2005). Visible light induced photocatalytic degradation of organic pollutants. *Journal of Photochemistry and Photobiology C: Photochemistry Reviews*, *6*(2-3), 186-205; https://doi.org/10.1016/j.jphotochemrev.2005.09.001.

[6] Augugliaro, V., Litter, M., Palmisano, L., & Soria, J. (2006). The combination of heterogeneous photocatalysis with chemical and physical operations: A tool for improving the photoprocess performance. *Journal of photochemistry and photobiology C: Photochemistry reviews*, *7*(4), 127-144; ttps://doi.org/10.1016/j.jphotochemrev.2006.12.001.

[7] Fujishima, A., & Honda, K. (1972). Electrochemical photolysis of water at a semiconductor electrode. *nature*, *238*(5358), 37-38;

[8] Warheit, D. B., Webb, T. R., Reed, K. L., Frerichs, S., & Sayes, C. M. (2007). Pulmonary toxicity study in rats with three forms of ultrafine-TiO_2 particles: differential responses related to surface properties. *Toxicology*, *230*(1), 90-104; https://doi.org/10.1016/j.tox. 2006.11.002.

[9] Gaya, U. I., & Abdullah, A. H. (2008). Heterogeneous photocatalytic degradation of organic contaminants over titanium dioxide: a review of fundamentals, progress and problems. *Journal of photochemistry and photobiology C: Photochemistry reviews*, *9*(1), 1-12; https://doi.org/10.1016 /j.jphotochemrev.2007.12.003.

[10] Romero, M., Blanco, J., Sánchez, B., Vidal, A., Malato, S., Cardona, A. I., & Garcia, E. (1999). Solar photocatalytic degradation of water and air pollutants: challenges and perspectives. *Solar energy*, *66*(2), 169-182; https://doi.org/10.1016/S0038-092X(98)00120-0.

[11] Schneider, J., Matsuoka, M., Takeuchi, M., Zhang, J., Horiuchi, Y., Anpo, M., & Bahnemann, D. W. (2014). Understanding TiO_2 photocatalysis: mechanisms and materials. *Chemical reviews*, *114*(19), 9919-9986; https://doi.org/10.1021/cr5001892.

[12] Ikezawa, S., Homyara, H., Kubota, T., Suzuki, R., Koh, S., Mutuga, F., & Famakinwa, T. (2001).

Applications of TiO_2 film for environmental purification deposited by controlled electron beam-excited plasma. *Thin Solid Films*, *386*(2), 173-176; https://doi.org/10.1016/S 0040-6090(00)01638-2.

[13] Xie, Y., Heo, S. H., Kim, Y. N., Yoo, S. H., & Cho, S. O. (2009). Synthesis and visible-light-induced catalytic activity of Ag_2S-coupled TiO_2 nanoparticles and nanowires. *Nanotechnology*, *21*(1), 015703; **DOI:** 10.1088/0957-4484/21/1/015703.

[14] Zheng, C., Qi, Z., & Chen, G. (2016). *Journal of the Textile Institute*, 107(12), 1501-1510; https://doi.org/10.1080/00405000.2015.1128227.

[15] Neves, M. C., Nogueira, J. M. F., Trindade, T., Mendonça, M. H., Pereira, M. I., & Monteiro, O. C. (2009). Photosensitization of TiO_2 by Ag_2S and its catalytic activity on phenol photodegradation. *Journal of Photochemistry and Photobiology A: Chemistry*, *204*(2-3), 168-173; https://doi.org/10.1016/j.jphotochem.2009.03.014.

[16] Grozdanov, I. (1995). Solution growth and characterization of silver sulfide films. *Applied Surface Science*, *84*(3), 325-329; https://doi.org/10.1016/0169-4332(94)00540-0.

[17] Tubtimtae, A., Wu, K. L., Tung, H. Y., Lee, M. W., & Wang, G. J. (2010). Ag_2S quantum dot-sensitized solar cells. *Electrochemistry Communications*, *12*(9), 1158-1160; https://doi.org/10.1016/j.elecom.2010.06.006.

[18] Liu, B., Wang, D., Zhang, Y., Fan, H., Lin, Y., Jiang, T., & Xie, T. (2013). Photoelectrical properties of Ag_2S quantum dot-modified TiO_2 nanorod arrays and their application for photovoltaic devices. *Dalton Transactions*, *42*(6), 2232-2237; DOI: 10.1039/c2dt32031b.

[19] Du, Y., Xu, B., Fu, T., Cai, M., Li, F., Zhang, Y., & Wang, Q. (2010). Near-infrared photoluminescent Ag_2S quantum dots from a single source precursor. *Journal of the American Chemical Society*, *132*(5), 1470-1471; https://doi.org/10.1021/ja909490r.

[20] Zhu, L., Meng, Z. D., & Oh, W. C. (2012). MWCNT-Based Ag_2S-TiO_2 Nanocomposites Photocatalyst: Ultrasound-Assisted Synthesis, Characterization, and Enhanced Catalytic Efficiency. *Journal of Nanomaterials*, *2012*(1), 586526; https://doi.org/10.1155/2012/58652 6.

[21] Lei, Z. H. U., Zeda, M. E. N. G., & Won-Chun, O. H. (2012). Hydrothermal synthesis of porous Ag_2S sensitized TiO_2 catalysts and their photocatalytic activities in the visible light range. *Chinese Journal of Catalysis*, *33*(2-3), 254-260; https://doi.org/10.1016/S1872-2067(10) 60296-3.

[22] Mossalayi, H., & Moghimi, A. (2011). Fabrication of TiO2/Ag2S nanocomposites via a new method for photocatalytic degradation of p-xylene & chlorophenol. *Journal of Chemical and Pharmaceutical Research*, *3*, 718-724.

[23] Oh, W. C., Zhang, F. J., & Chen, M. L. (2010). Synthesis and characterization of V–C60/TiO_2 photocatalysts designed for degradation of methylene blue. *Journal of Industrial and Engineering Chemistry*, *16*(2), 299-304; https://doi.org/10.1016/j.jiec.2009.09.065.

[24] Bourlinos, A. B., Gournis, D., Petridis, D., Szabó, T., Szeri, A., & Dékány, I. (2003). Graphite oxide: chemical reduction to graphite and surface modification with primary aliphatic amines and amino acids. *Langmuir*, *19*(15), 6050-6055; https://doi.org/10.1021/la0 26525h.

[25] Arunkumar, T., & Shanthi, M. (2024). *J. Chem. Health Risks,* 14(3), 1461-1481.

[26] Yang, M., Hume, C., Lee, S., Son, Y. H., & Lee, J. K. (2010). Correlation between photocatalytic efficacy and electronic band structure in hydrothermally grown TiO_2 nanoparticles. *The Journal of Physical Chemistry C*, *114*(36), 15292-15297; https://doi.org/10.1021/jp10 3764n.

[27] Pan, S., & Liu, X. (2012). ZnS–Graphene nanocomposite: Synthesis, characterization and optical properties. *Journal of Solid State Chemistry*, *191*, 51-56; https://doi.org/10.1016/j.jss c.2012.02.048.

[28] Nasrollahzadeh, M., Atarod, M., Jaleh, B., & Gandomirouzbahani, M. (2016). In situ green synthesis of Ag nanoparticles on graphene oxide/TiO2 nanocomposite and their catalytic activity for the reduction of 4-nitrophenol, Congo red and methylene blue. *Ceramics International*, *42*(7), 8587-8596; https://doi.org/10.1016/j.ceramint.2016.02.088.

[29] Krishnakumar, B., Selvam, K., Velmurugan, R., & Swaminathan, M. (2010). Influence of operational

parameters on photodegradation of Acid Black 1 with ZnO. *Desalination and Water Treatment*, *24*(1-3), 132-139; https://doi.org/10.5004/dwt.2010.1466.

[30] Jayamani, G., & Shanthi, M. (2020). An efficient nanocomposite CdS-$ZnWO_4$ for the degradation of Naphthol Green B dye under UV-A light illumination. *Nano-Structures & Nano-Objects*, *22*, 100452; https://doi.org/10.1016/j.nanoso.2020.100452.

[31] Kartal, Ö. E., Erol, M., & Oğuz, H. (2001). Photocatalytic destruction of phenol by TiO_2 powders. *Chemical Engineering & Technology: Industrial Chemistry-Plant Equipment-Process Engineering-Biotechnology*, *24*(6), 645-649; https://doi.org/10.1002/1521-4125(200106)24:6%3C645::AID-CEAT645%3E3.0.CO;2-L.

[32] Okamoto, K. I., Yamamoto, Y., Tanaka, H., Tanaka, M., & Itaya, A. (1985). Heterogeneous photocatalytic decomposition of phenol over TiO_2 powder. *Bulletin of the Chemical Society of Japan*, *58*(7), 2015-2022; https://doi.org/10.1246/bcsj.58.2015.

[33] Pichat, P., Guillard, C., Amalric, L., Renard, A. C., & Plaidy, O. (1995). Assessment of the importance of the role of H_2O_2 and $O_2^{\bullet-}$ in the photocatalytic degradation of 1, 2-dimethoxybenzene. *Solar energy materials and solar cells*, *38*(1-4), 391-399; https://doi.org/10.1016/0927-0248(94)00231-2.

[34] Bekbölet, M., Lindner, M., Weichgrebe, D., & Bahnemann, D. W. (1996). Photocatalytic detoxification with the thin-film fixed-bed reactor (TFFBR): clean-up of highly polluted landfill effluents using a novel TiO_2-photocatalyst. *Solar Energy*, *56*(5), 455-469; https://doi.org/10.1016/0038-092X(96)00020-5.

[35] Pelizzetti, E., Carlin, V., Minero, C., & Grätzel, M. (1991). Enhancement of the rate of photocatalytic degradation on TiO_2 of 2-chlorophenol, 2, 7-dichlorodibenzodioxin and atrazine by inorganic oxidizing species. *New journal of chemistry (1987)*, *15*(5), 351-359.

[36] Shanthi, M., & Kuzhalosai, V. (2012). Photocatalytic degradation of an azo dye, Acid Red 27, in aqueous solution using nano ZnO.

[37] Chen, L. C., & Chou, T. C. (1993). Kinetics of photodecolorization of methyl orange using titanium dioxide as catalyst. *Industrial & engineering chemistry research*, *32*(7), 1520-1527; https://doi.org/ 10.1016/0304-5102(93)80102-Z.

[38] Wenhua, L., Hong, L., Suoan, C., Jianqing Z., & Chunan, C. (2000). Kinetics of photocatalytic degradation of aniline in water over TiO_2 supported on porous nickel. *Journal of Photochemistry and Photobiology A: Chemistry*, 131(1-3), 125-132; https://doi.org/10.1016/S1010-6030(99)00232-4.

[39] Alaton, I. A., & Balcioglu, I. A. (2001). Photochemical and heterogeneous photocatalytic degradation of waste vinylsulphone dyes: a case study with hydrolyzed Reactive Black 5. *Journal of Photochemistry and Photobiology A: Chemistry*, *141*(2-3), 247-254; https://doi.org/10.1016/S1010-6030(01)00440-3.

[40] Sharma, A., Rao, P., Mathur, R.P., & Ametha, S.C. (1995). *Journal of Photochemistry and Photobiology A: Chemistry*, 86(1-3), 197; https://doi.org/10.1016/1010-6030(94)03933-L.

[41] Subash, B., Krishnakumar, B., Swaminathan, M., & Shanthi, M. (2013). Highly efficient, solar active, and reusable photocatalyst: Zr-loaded Ag–ZnO for reactive red 120 dye degradation with synergistic effect and dye-sensitized mechanism. *Langmuir*, *29*(3), 939-949; https://doi.org/10.1021/la303842c.

[42] Chen, C., Xie, Y., Ali, G., Yoo, S. H., & Cho, S. O. (2011). Improved conversion efficiency of Ag_2S quantum dot-sensitized solar cells based on TiO_2 nanotubes with a ZnO recombination barrier layer. *Nanoscale research letters*, *6*, 1-9; http://www.Nanoscalereslett. com/content/6/1/462.